



PAS
02 JUL 29 2002
INCOMING

MEMORANDUM FOR: SAF/PAS
1690 Air Force Pentagon - 5D227
Washington DC 20330-1690

JUL 23 2002

FROM:


Francis G. Hinnant, Col, USAF
Associate Director of Acquisition
NPOESS Integrated Program Office
8455 Colesville Rd, Suite 1450
Silver Spring, MD 20910

02 - 0484
Call 697-3222/697-8932
for pickup or return to 5D227

SUBJECT: Paper approval for: Scene Generation Studies in Support of the Next-Generation of Polar Orbiting Low-Light Imagers

Enclosed are the required ten (10) copies of the subject papers. This paper will be published in a publication entitled "Remote Sensing of the Environment". It was written by ITT Industries and Ball Aerospace Corporation.

The program office has reviewed the information in the attached papers and found it appropriate for public disclosure without change.

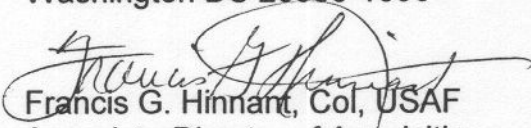
Point of contact on this matter is Jeffrey Dedrick, NPOESS IPO at 301-427-2084 (Ext. 212).

Attachment: Paper—10 copies



MEMORANDUM FOR: SAF/PAS
1690 Air Force Pentagon - 5D227
Washington DC 20330-1690

JUL 23 2002

FROM: 
Francis G. Hinnant, Col, USAF
Associate Director of Acquisition
NPOESS Integrated Program Office
8455 Colesville Rd, Suite 1450
Silver Spring, MD 20910

SUBJECT: Paper approval for: Scene Generation Studies in Support of the Next-Generation of Polar Orbiting Low-Light Imagers

Enclosed are the required ten (10) copies of the subject papers. This paper will be published in a publication entitled "Remote Sensing of the Environment". It was written by ITT Industries and Ball Aerospace Corporation.

The program office has reviewed the information in the attached papers and found it appropriate for public disclosure without change.

Point of contact on this matter is Jeffrey Dedrick, NPOESS IPO at 301-427-2084 (Ext. 212).

Attachment: Paper—10 copies

Scene Generation Studies in Support of the Next-Generation of Polar Orbiting Low-Light Imagers

George D. Modica*, Edward J. Kennelly, John Evans , Robert P. d'Entremont,
Gary B. Gustafson

*Atmospheric and Environmental Research, Inc.
131 Hartwell Ave.
Lexington, MA 02421*

David E. Flittner

*Dept. of Atmospheric Sciences, University of Arizona
Tucson, Arizona*

Neil Endsley

*Ball Aerospace Corporation
Boulder, Colorado*

5 October 2001

* Corresponding author address: George D. Modica, AER, Inc., 131 Hartwell Ave., Lexington, MA 02421-3126. Email: gmodica@aer.com
Current affiliation: University of Maine

ABSTRACT

We describe a process to synthesize satellite imagery that exhibits characteristics similar to what might ultimately become available from the nighttime visible band of the next-generation of polar-orbiting imager instruments. The process begins by creating a modeled scene that includes a realistic terminator—the region where the magnitude of the top-of-atmosphere radiance is a strong function of the solar zenith angle. The terminator is accurately modeled by first obtaining data from a spherical coordinate multi-scattering radiative transfer model. Only the moon in quarter-phase illuminates the nighttime side of the terminator. After this data is applied to the scene, the effects of instrument motion blur, resampling, noise, etc. are parameterized and introduced into the image through the use of a simple sensor effects model. The simulated terminator imagery is used to test a Near Constant Contrast (NCC) algorithm that is supposed to produce an image in which, among other things, the contrast of scene features does not vary noticeably anywhere along a line transiting the terminator. The NCC product generated by this algorithm compares favorably with the original ground truth image used as the basis for the modeled terminator scene in terms of feature validation achieved through a manual analysis of the imagery. This exercise raises the level of confidence in the capability of a prospective NPOESS nighttime visible band instrument to provide data that will satisfy user-driven requirements and be of great benefit to operational and research meteorology.

1. Introduction

The launch of the first Television Infrared Observation Satellite (TIROS) was the United States' first experimental milestone to determine the usefulness of satellites to study the earth. Over forty years later, the role that weather satellites fulfill has never been greater and new systems continue to be designed, developed, and launched into service. On the 40th anniversary of TIROS, it is appropriate to recount a few of the environmental issues that have benefited as a result.

Recognizing the crucial role that clouds play in global climate, researchers have relied on cloud and ice analyses derived from satellite image data to provide clues to the mysteries of global-climate change. Population growth and “urban sprawl” are objectively monitored by examination of time series satellite data of city lights. Satellite imagery also provides a real-time means of monitoring man-made and natural fires, natural gas field flaring, land use, severe weather, and aurora to name a few.

The current inventory of operational polar-orbiting imaging satellites that have contributed to these achievements each have their roots in programs from one or more of three agencies: NASA, NOAA, and the Defense Meteorological Satellite Program (DMSP). NASA, e.g., has led the development of the Landsat Thematic Mapper (Tokola et al. 1999). This is a multispectral imager that provides high spatial resolution information on land use. It has a horizontal spatial resolution of 30 m at nadir. More recently, NASA launched the Moderate Resolution Imaging Spectroradiometer (MODIS), which acquires imagery at up to 250 m resolution for a much wider swath width than Landsat. The Advanced Very High Resolution Radiometer (AVHRR; Rao et al. 1990) sponsored by NOAA is a 5 channel scanning radiometer with 1.1 km resolution. The DMSP Operational Line Scan (OLS; Kroehl et al. 1994) is another imaging instrument that consists of two telescopes: one for the visible band and one for IR, each

having 0.55 km horizontal spatial resolution. The OLS includes a nighttime visible capability—something not present aboard the civilian platforms—having 2.7 km horizontal spatial resolution and is made possible through the use of photo-multiplier tube (PMT) technology. The PMT is sensitive to very low levels of light in the 0.47-0.95 μm band, enabling detection of meteorological features with as little as half-moonlight illumination. The nighttime visible imaging feature of the OLS is important for extending visible-band analysis capability into non-daylight hours. While IR channel data is essential for nighttime viewing, under certain conditions (e.g., strong temperature inversions, transmissive clouds) image features can be more difficult to interpret. In fact, the nighttime visible band data is so useful that it was added to the requirements for the National Polar-orbiting Operational Environmental Satellite System (NPOESS), which is discussed in Section 2. It is our interest in the “low-light” imaging requirement of NPOESS that motivated this study. Having the ability to experience beforehand the imagery characteristics provided by a new low-light instrument is, of course, desirable in itself. But it is also an essential component in the design phase of an imaging instrument as it not only affords potential users of the data the opportunity to test and refine ahead of time algorithms that might potentially use the data, but assists the instrument designers as well. In Section 3 we present a methodology to generate the desired imagery product followed by a discussion in Section 4 of the results produced by an algorithm that used the imagery.

2. NPOESS

NPOESS combines the country’s civilian and military weather polar-orbiting satellite programs into a single system. NPOESS is currently in the development phase and will begin to provide data operationally in the 2005-2008 time frame. There are 6 NPOESS payloads currently under development: the Visible/IR Radiometer Suite (VIIRS), the Cross-track IR Sounder (CrIS), the Conical Microwave Imager/Sounder (CMIS), the Ozone Mapper/Profiler Suite (OMPS), the GPS Occultation Sensor (GPSOS), and the Space Environmental Sensor Suite (SESS). NPOESS is intended to provide *operational* remote sensing capability to acquire and receive environmental data in real-time. The data will be acquired at field terminals and acquired, stored, and disseminated at processing centers. The environmental data will consist of global and regional imagery, specialized meteorological, climatic, terrestrial, oceanographic, and solar geophysical data in support of both civilian and national security missions.

A key strategy of NPOESS is to optimize the development of critical sensor payloads through the unprecedented participation of the algorithm developer in the sensor design process. Rather than develop algorithms *after* the instruments have been designed, algorithm developers are involved in all phases of instrument development: requirements analysis, design, testing, and evaluation of the sensors, measuring performance against end-user requirements each step of the way. Algorithm development is primarily driven by formal NPOESS specifications, which include requirements for the system to produce specific Environmental Data Records (EDRs). EDRs are data that contain the measured environmental parameters or imagery as well as any ancillary data required to identify or to interpret these parameters or images. EDRs are generally produced through the application of one or more algorithms to the Sensor Data Records (SDRs) and must meet specific content, quality, reporting frequency, and timeliness requirements.

The Near Constant Contrast (NCC) product is one of the required components of the VIIRS Imagery EDR. The NCC product is defined as imagery derived from a daytime/nighttime spectral band provided by VIIRS and which maintains apparent feature contrast under daytime, nighttime, and terminator conditions. Some NCC requirements to note are those for the largest permissible pixel dimension, or Horizontal Spatial Resolution (HSR), and the Horizontal Reporting Interval (HRI). The threshold values for these are specified as 2.6 km and “gapless” coverage, respectively, with the latter requiring that $HSR \geq HRI$. The swath width requirement is 3000 km. The daytime/nighttime visible band is required to have a dynamic range of at least 4.0×10^{-9} $3.0 \times 10^{-2} \text{ Wcm}^{-2}\text{sr}^{-1}$ in the $0.4 - 1.0 \mu\text{m}$ band, or equivalent in another band. This implies that the daytime/nighttime visible band must be capable of providing useful imagery down to about quarter-phase lunar illumination. By far, the most stressing case to consider for NCC product generation is one where the terminator is present in the scene. As we shall see in Section 4, the top-of-atmosphere (TOA) radiance across the terminator is characterized by a range of many orders of magnitude. This creates a challenge for both sensor design and display. In order to develop and test a NCC algorithm under such conditions, it would be useful to have actual imagery from the terminator. Again, this is problematic for reasons that will be made clear later. Our solution is to synthesize a terminator scene through a series of modeling steps that are described in the next section.

3. Methodology

The method we used to generate the NCC product consists of four basic steps: 1) Acquire data from a radiative transfer model (RTM) that can accurately model the TOA radiance in the vicinity of the terminator; 2) apply the model data to the generation of the terminator scene; 3) transform the scene in order to parameterize the most relevant low-light instrument characteristics; 4) generate the NCC product.

a. RTM terminator studies

A collection of satellite imagery data from the terminator region would be invaluable for trade studies in support of the NCC product. However, there currently does not exist a definitive source of terminator radiance data upon which to rely for our purposes. One prospective source of military data is the DMSP OLS, which includes a PMT instrument for measurement of low radiance data. However, data from neither the OLS nor PMT are strictly calibrated, making them unsatisfactory for accurate simulations of the low-light data and ultimate instrument design. AVHRR and TM do not have sufficient dynamic range characteristics to provide accurate data at very low light levels. Another option is to utilize simulated data in lieu of remotely sensed data. For example, MODTRAN (version 4.0) could be used to simulate TOA radiances. There would, however, be a logistical problem of making costly MODTRAN calculations at the millions of points (pixels) that make up an image. Furthermore, while MODTRAN does include refractive spherical geometry in some of its calculations, it relies on plane-parallel atmosphere assumptions for the calculation of multi-scattering effects. At low solar zenith angles ($85^\circ \leq \text{SZA} \leq 105^\circ$) this effect would contribute to unacceptable levels of total TOA radiance error, thereby rendering MODTRAN-based terminator scenes inadequate for our purposes. In consideration of this, we chose to acquire data from a spherical coordinate multi-scattering RTM appropriate for computing reflected TOA radiance at high solar zenith

angles (Herman et al.1995). In this model, the atmosphere is divided into homogenous spherical shells. The intensity at any point is a function of five independent variables (3 for location and 2 for the direction of radiation). The model parameterizes the effects on radiative transfer of aerosol scattering, gaseous and aerosol absorption, and in more recent versions, polarization. For each shell, the model uses an integrated form of the general radiative transfer equations and computes all distances and angles by assuming spherical geometry.

Previous tests of this model indicated it is accurate to better than 1% for most Earth-atmosphere situations. When compared with “flat” or plane parallel atmospheric models, differences > 10% were found in the transmitted intensities at the surface for all lines of sight when the SZA was greater than 85° and spherical effects were neglected. For an optical depth of 0.5, a SZA > 80°, and view angles within 10% of the horizon, spherical effects must be included to avoid errors greater than 5%. For a SZA of 85°, errors of 5% were found for optical depths as small as 0.1. Other comparisons of the spherical geometry model with the flat model confirm the need to include spherical effects when examining the intensity field at the top of the atmosphere.

We used this model to expose some of the performance implications of a visible band low-light sensor that images from a low earth orbit (~833 km) in the vicinity of the terminator. For this study, the RTM was used to estimate effective TOA normalized (I/F) scene reflectance as a function of the conditions specified below in Table 1. Table 2 lists the surface parameters used in the model. The results from the RTM are generally consistent with earlier Air Force data that describe the drop in TOA radiance with increasing SZA at OLS/PMT visible wavelengths (Figure 1). Some quantitative differences between the OLS and RTM curves were bound to occur due to assumptions on the control parameters listed below. Nevertheless, it will be invaluable from the standpoint of both algorithm and instrument design if the RTM can be used to provide quantitative guidance on the nature of scene radiances in the vicinity of the terminator.

Table 1. Satellite and solar geometry parameters

Parameter	Value
Wavelengths ¹ (nm)	469
	542
	645
	858
Solar Zenith (deg)	105
	100
	95
	90
	85
Satellite Zenith (deg)	0
	45
	70
Azimuth ² (deg)	0 to 150 (every 30 deg)
	150-180 (every 5 deg)

¹Wavelengths selected to match center wavelengths of VIIRS bands.

² Azimuth angle convention is such that 180° indicates sensor looking directly toward sun, 0° is satellite directly between sun and viewed point.

Table 2. Surface type parameters

Surface Type	Reflectance				Altitude (km)
	469 nm	542 nm	645 nm	858 nm	
vegetated land	0.07	0.10	0.07	0.40	0
ocean	BRDF	BRDF	BRDF	BRDF	0
cloud	0.70	0.70	0.65	0.65	2

b. Input scene selection

Unfortunately, VIIRS imagery will not be available for several more years. In order to test VIIRS algorithms in the meantime, the VIIRS imagery must be approximated. In making these approximations, several important issues must be addressed.

The first issue in scene approximation or generation is that it is necessary to include the effect the sensor instrument has on the imagery. The instrument's electronic, optical, and mechanical components combine in characteristic ways to introduce artifacts into an image. Some of these sensor characteristics are commonly known as sensitivity, noise, out of field effects, spatial smoothing, and distortion. Any attempts to approximate VIIRS imagery must account for and include these effects. The effects can be simulated with the use of a sensor model that can parameterize these characteristics to approach the VIIRS specifications. A second issue is the attenuation of radiances from clouds (water and/or ice) and by the intervening atmosphere. This effect has scan angle dependence, since the imager will view through a longer optical path at higher scan angles. A third complication arises when simulating cloud and ice features: Synthetic data with realistic spatial detail are extremely difficult to produce. In contrast to automated algorithms, analysts rely primarily on spatial—as opposed to radiometric—characteristics to interpret a scene. While radiative transfer models do exist to simulate accurately the radiometric characteristics of simplified cloud and terrestrial surfaces, the process of modeling scenes having complicated spatial features presents a much greater challenge.

The solution we adopted was to use a combination of high-resolution image data and sensor effects modeling (see below) as the basis for establishing our synthetic scene. This approach ignores the radiometric dependence on scan angle mentioned in the second consideration above, but for manual analysis applications where radiometric accuracy is not strictly required, this drawback is of second order importance. Of the imager platforms mentioned in Section 1, the AVHRR instrument aboard the NOAA polar-orbiting satellites was the most readily obtainable. While its horizontal spatial resolution is significantly less than that of Landsat, (1.1 km vs. 30 m at nadir) AVHRR provides a much larger swath width (2400 km vs. 185 km)—a useful advantage for simulating a scene that includes the full extent of the terminator region.

c. Terminator scene generation

In order to test the NCC product algorithm with imagery it will be necessary to collect candidate terminator scenes for input. As discussed earlier, obtaining real data for this purpose is problematic. However, we may use the RTM data to generate artificial terminator scenes by modulating the observed top-of-atmosphere (TOA) radiances from AVHRR *daytime* scenes, such that the resulting values decrease with increasing SZA in accordance with one of the curves from Figure 1. For this we selected a mid-afternoon AVHRR scene from September 1999 (Figure 2). The original field of SZA in this scene was replaced with values consistent with a terminator in the center of the scene. The next step was to modulate the TOA radiance values at every pixel to be consistent with the RTM curves for AVHRR channels 1 and 2. Model parameters appropriate for an assumed vegetation-covered surface (Table 2) were used. Since we had data from the RTM model at only five solar zenith angles from 85° to 105°, we interpolated the data with a cubic spline function to a lookup table at every 0.01 SZA degree. Next, we normalized the RTM curves so that the normalized radiance = 1 for SZA = 85°, essentially creating a table of weights as a function of SZA. Then, the radiance in the terminator scene (R_{term}^{ij}) was computed according to

$$R_{term}^{ij} = R^{ij} \cdot w(SZA), \quad (1)$$

where i, j are the indexes in the image x, y directions, respectively; R^{ij} is the initial AVHRR scene radiance; $w(SZA)$ are the weights obtained from the above look-up table.

Figure 2 shows the AVHRR scene used to provide R^{ij} . This image covers an area over the northeast United States and Atlantic Ocean. Some identifiable surface features in this image are the New England coastline and much of Long Island. The St. Lawrence River (with Lake Champlain to the south) may be identified near the top of the image, leading to its source—Lake Ontario—in the upper left. A variety of low-, mid-, and upper-level clouds cover much of the western edge and center of the image; clusters of clouds are also apparent over the Atlantic Ocean, with fog off of the coast of Maine. The field of R_{term}^{ij} , after application of the RTM curves to the AVHRR channel 2 data, is shown in Figure 3. Note that despite the apparent lack of identifiable features in much of the scene, there are in fact radiance variations. The scene radiances fall to about $9 \times 10^{-9} \text{ Wcm}^{-2}\text{sr}^{-1}$ in the 0.46 – 0.86 μm band (see below) over the darkest portion of the scene.

d. Spectral matching

The spectral resolution of the low-light band (assumed here to be 0.46 – 0.86 μm) is relatively broad with respect to the AVHRR channels in the same range (0.58-0.68 μm for channel 1 and 0.725-1.10 μm for channel 2). We may combine narrower band image data to produce a broader band image by using a spectral matching technique:

$$\bar{R} = \frac{\sum_{i=1}^2 a_i R_i}{\sum_{i=1}^2 a_i} \quad (2)$$

where R_i are the AVHRR channel radiances and a_i are weighting coefficients. The coefficients a_i were specified to be proportional to the AVHRR 50% power half-bandwidths. AVHRR channels 1 and 2 were used in Eq. 2.

e. Simple sensor effects model

There are many attributes of an image sensor that are important for image quality. The optics, mechanics (including properties of the orbit), and electronics of the imaging system can affect these attributes. Since our goal is to generate the most realistic NCC product as is reasonably possible, the synthesized scene used as input for the NCC algorithm ought have characteristics that are consistent with the low-light imager. We used a simple sensor effects model (SSEM) to do this. The SSEM includes parameterizations of the following effects:

- Horizontal Spatial Resolution (HSR)—a measure of the “sharpness” of the imagery. In the SSEM, this is determined by a choice of a system modulation transfer function (MTF), which is the Fourier transform of the end-to-end system point spread function (PSF). The SSEM includes the option to use different shaped PSFs (e.g., square, Gaussian);
- Horizontal Reporting Interval (HRI)—the ground space distance between neighboring points in the horizontal at which imagery is estimated and reported. Various combinations of under- or oversampling may be tested. For reasons that are beyond the scope of this paper, we selected an NCC grid having a 1.47 x 1.47 km pixel dimension to satisfy the HSR and HRI requirements.
- Noise—artifacts introduced into an image due to system imperfections. Noise affects the uniformity of the target and background and the potential for differentiating between them (i.e., contrast). Sources can be coherent (correlated) and incoherent (random, e.g., white noise). This also includes quantization noise, which arises from the discretization of the dynamic range of an instrument as determined by the number of bits used to quantify the radiance. Noise models developed for the VIIRS low-light instrument were utilized in the sensor simulation.

The simple sensor effects model is not intended to be a substitute for rigorous modeling of all sensor system effects. The formal design process of the low-light visible band instrument included the development of a sophisticated sensor system model that explicitly represents every component of the imaging system. However, the SSEM ensures that the most stressing low-light band image quality effects are accounted for. These are pixel aspect ratio, MTF, and HRI. While the original AVHRR scene (Figure 2) used as input to the SSEM includes its own unique sensor artifacts, we believe these do not detract from the results in this study for the following reasons: Most importantly, the NCC product is not a radiometric product at all, since there has to be a transformation from radiance space to “gray-shade” space during contrast adjustment (see Section f below). Were we primarily interested in the absolute radiometry of the low-light band, we would have to be more sensitive to the AVHRR sensor effects. Secondly, the AVHRR and low-light band pixel sizes at nadir are smaller than the 1.47 x 1.47 km pixel

dimension of the NCC grid. Minimally detectable spatial features that would be most affected by characteristic AVHRR sensor effects will be all but lost when sampled to the NCC grid.

Figure 4 shows the scene in the sensor coordinates of the low-light imager. The figure presents the results from two cases: The top figure shows the view based on the shape of low-light band pixels at nadir, while the lower figure shows the scene is based on edge of field shaped pixels. The reason the aspect ratio of the scenes differs from that in the original (Figure 3) is because of the low-light sensor pixel shape, which at nadir is rectangular, with the along-track dimension about three times the cross-track value. At edge of field (1500 km from nadir) and since this particular sensor design was a push-broom type instrument, the pixel aspect ratio changes to one having a cross-track width twice that of the down-track length. These characteristics were based on an 833 km altitude orbit.

f. Contrast adjustment

Since nighttime visible imagery band data can span a very large dynamic range (over seven orders of magnitude; see Figure 1), visual display of the data presents a challenge because common display techniques are best suited to viewing data that typically spans no more than two orders of magnitude. To meet requirements, a contrast normalization data processing step is necessary to ensure that the NCC data will be presented in a way that ensures adequate contrast across all radiance levels expected in the image. The contrast normalization is most effectively carried out locally, i.e., over a subset of the entire image to accommodate the potentially wide dynamic range of scene radiances. An adaptive algorithm whose parameters change from pixel to pixel according to the image contrast of local, or neighboring pixels may be used to achieve the desired enhancement. One such algorithm has been described in Schowengerdt 1997, and is known as Local Range Modification (LRM). The algorithm partitions the image spatially into adjoining bins. Due to the fact that the brightness intensity of the image can be a strong function of SZA (Figure 1), we modified the LRM algorithm to align the long axis of each bin parallel to lines of constant SZA. The bin dimensions are adjustable: The bin width is selected as a function of the SZA and the bin length as a function of the image (height) dimension. The algorithm next computes a contrast stretch unique to each pixel. This stretch is dependent on the local contrast within bin n ($n = 1, 2, 3, \dots, N$ number of bins per image):

$$GL_{i,j}(n) = 255 * \frac{(DN_{i,j} - DN_{\min})_n}{(DN_{\max} - DN_{\min})_n} \quad (3)$$

where $GL_{i,j}(n)$ is the gray level for pixel i,j within bin n , $DN_{i,j}$ is the digital number of pixel i,j , and $(DN_{\min} - DN_{\max})_n$ is the digital number range in bin n . Here, we assume the display ranges from $[0, 255]$ gray shades.

4. Results and Discussion

a. Qualitative aspects of the NCC product

The NCC product is shown in Figure 5. The nadir image in Figure 4 was used as input to the NCC product algorithm. The NCC algorithm regrid the image from the low-light instrument scan projection of Figure 4 to the 1.47 km NCC product grid and performs the contrast adjustment with Eq. 3. There were few noticeable differences between the nadir NCC product and a second one (not shown) that used edge of field-shaped pixels. A comparison of the NCC product with the original AVHRR terminator scene in Figure 3 reveals that the most obvious difference is in features within the “nighttime” region; clouds and surface features are now readily identifiable in the NCC product, as they are in the original AVHRR image (Figure 2). A closer look also supports the claim that the contrast is not a function of position with respect to the terminator. However, Figure 5 does present an example of how artifacts can be introduced into the image by the LRM algorithm. In the northeast corner of Figure 5 in the vicinity of the St. Lawrence River, some of the bin boundaries are noticeable. These appear as striping oriented northwest-southeast in the image. The striping is caused by the tendency of the LRM technique to distribute the contrast in a bin across all [255] gray shades even when there isn’t much contrast to begin with (i.e., the denominator in Eq. 3 is small). Unfortunately, without supporting information such as snow cover analysis, or some other meteorological guidance, this artifact could be misinterpreted as cloud or snow cover. To a lesser extent, bin boundaries are also evident over the Atlantic Ocean, south of Long Island. It should be noted here that the NPOESS user workstations would likely be configured with a wide variety of supporting databases to assist in the identification of features of interest. Furthermore, in an operational setting at a field terminal, a user likely would be able to manipulate easily the choice of bin size used in the LRM algorithm. In fact, tests have revealed that with a little trial and error, undesirable artifacts in the NCC product can be minimized to an acceptable level for manual applications. Lastly, future versions of the NCC algorithm itself could include refinements that will minimize the introduction of artifacts for those regions in the scene having little contrast.

b. Quantitative aspects of the NCC product

The NCC product was intended to provide users with an additional nighttime information source for analyzing imagery. In order to guarantee that sufficiently high quality imagery will be available from the low-light band sensor aboard VIIRS, both instrument and algorithm designers must demonstrate that this imagery meets certain threshold requirements. As mentioned in Section 2, certain of these requirements are applicable to the content, quality, reporting frequency, and timeliness of the imagery; others pertain to specific, manually derived products that are based upon the imagery. Some examples of the latter are cloud cover fraction, cloud type, sea ice concentration, and sea ice edge location. These products can be derived using any combination of VIIRS imagery bands, display enhancements, and additional supporting databases, such as geography. The requirements for the manually derived cloud cover fraction product are shown in Table 3. These and other requirements are detailed in a Systems Requirements Document issued by the NPOESS Integrated Product Office.

Parameter	Thresholds	Objectives
a. Horizontal Cell Size	3 times the Imagery HSR	2 times the Imagery HSR
b. Horizontal Reporting Interval	Horizontal cell size	Horizontal cell size
c. Measurement Range	0 - 1, 0.1 increments	0 - 1, 0.1 increments
d. Measurement Uncertainty	0.1	0.1

Table 3. Requirements for manually the derived cloud cover fraction product

The Horizontal Cell Size (HCS) in Table 3 refers to the areal extent of an image sample in which we wish to measure cloud fraction. In this case, the HCS is defined as “3 times the [VIIRS] Imagery HSR,” which is 3 times 400 m, or 1.2 km. Therefore, the problem becomes one of determining the fraction of a $(1.2 \text{ km})^2$ area covered with cloud. The Horizontal Reporting Interval (HRI) specifies how frequently (in space) the cloud fraction is to be reported. In this case, the HRI is equal to the HCS. This implies the analyzed cells must be contiguous. The Measurement Range specifies the interval at which the cloud fraction must be analyzed (i.e., 0, 0.1, 0.2,1.0). Finally, the Measurement Uncertainty is a measure of error and indicates how far the manually derived cloud fraction departs the actual, or truth value. The measurement uncertainty is defined as

$$\xi_N = \left[\sum_{i=1}^N (x_i - x_T)^2 / N \right]^{1/2}, \quad (4)$$

where x_i is the value obtained in the i th estimate of the parameter, and x_T is the truth value of the parameter. The value of ξ_N is required to be ≤ 0.1 . It is important to note that the NCC product does not by itself have to meet the measurement uncertainty requirement given in Table 3; rather, a manual analysis may be derived from any or all of the imagery channels. These include daytime visible and thermal infrared channels having 400m HSR (nadir).

Since we are interested in learning some of the characteristics of the NCC product, we computed the cloud fraction measurement uncertainty as defined in Eq. 4 based only on the NCC product shown in Figure 5. We used the following procedure to enable us to make this calculation: First, we produced a manual cloud analysis from the NCC product image shown in Figure 5 to yield a cloud mask. For this we utilized a “threshold blanking” utility that permits adjusting downward the intensity of the background over some subset of the full scene until only the target (e.g., the clouds) remains. The subset area is saved, and the process is repeated until the entire scene is covered. The result is a yes/no cloud mask for each pixel of the NCC product. A second manual cloud analysis from a similar procedure was produced by using the full (5) channel set of the higher spatial resolution AVHRR “truth” image shown in Figure 2. In this case, we also utilized visualization tools that permitted multispectral enhancement of the truth imagery. Note that we generated the NCC product cloud mask *before* the truth mask, so as not to prejudice the former. Since the AVHRR data and NCC product exist on different grid projections (AVHRR is in scan projection and the NCC product is on a $1.47 \times 1.47 \text{ km}$ grid), the third step in the processing required remapping the cloud masks from each analysis to a common grid. We selected for this test a Lambert Equal Area map

projection. The remapped cloud masks from the truth analysis and NCC product are shown in Figure 6. Finally, Eq. 4 was applied to the data in Figure 6 to calculate the measurement uncertainty. In this test, we obtained a measurement uncertainty value of 0.23. While this is certainly greater than the threshold value of 0.1 given in Table 3, it is reasonable after considering that the manual cloud fraction analysis used no sources of information other than the NCC product. During the test phase of VIIRS we routinely achieved the threshold requirement for cloud cover measurement uncertainty when the higher spatial and spectral resolution VIIRS imagery data were available.

In this study, we simulated imagery from an as-yet-to-be-built low-light band satellite sensor as a means of supporting the risk reduction activities during the design phase of the NPOESS VIIRS program. The simulated imagery exhibits the essential characteristics we expect to see in real satellite data. We used this simulated imagery to test an NCC product algorithm, which must be capable of displaying features down to quarter-phase lunar illumination conditions. A quantitative assessment of the NCC product suggests that it will be an invaluable component in cloud (or ice) analysis, not to mention climate, land use studies, and other applications.

Acknowledgments. This effort was supported by the NPOESS Integrated Project Office through a contract with ITT Defense and Electronics.

REFERENCES

- Herman, B., T.R. Caudill, D.E. Flittner, K.J. Thome, and A. Ben-David, 1995: Comparison of the Gauss-Seidel Spherical polarized radiative transfer code with other radiative transfer codes. *J. Appl. Optics*, **34:13**, 4563-4572.
- Kroehl, H.W., G.R. Scharfen, E.S. Arrance, and S.J. Goodman, 1994: Archive of digital data from the Defense Meteorological Satellite Program (DMSP). *Tenth International Conference on Interactive Information and Processing Systems for Meteorology, Oceanography, Hydrology*, January 23-28, Nashville, TN, American Meteorological Society.
- Rao, P.K., S.J. Holmes, R.K. Anderson, J.S. Winston, and P.E. Lehr, 1990: *Weather Satellites: Systems, Data, and Environmental Applications*. American Meteorological Society, Boston, ISBN 0-933876-66-1.
- Schowengerdt, R.A., 1997. *Remote Sensing: Models and Methods for Image Processing*. 2nd ed. San Diego, CA: Academic Press, 522 p.
- Tokola, T., S. Löfman, and A. Erkkilä, 1999: Relative calibration of multitemporal Landsat data for forest cover change detection. *Rem. Sens. Env.*, **68:1**, 1-11.

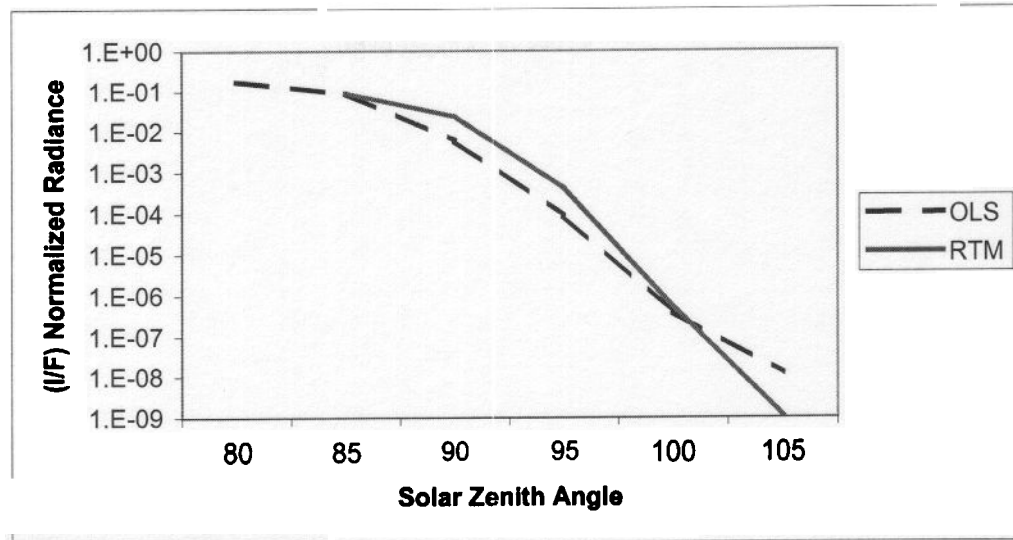


Figure 1. Normalized scene radiance as a function of solar zenith angle for OLS and the radiative transfer model (RTM)

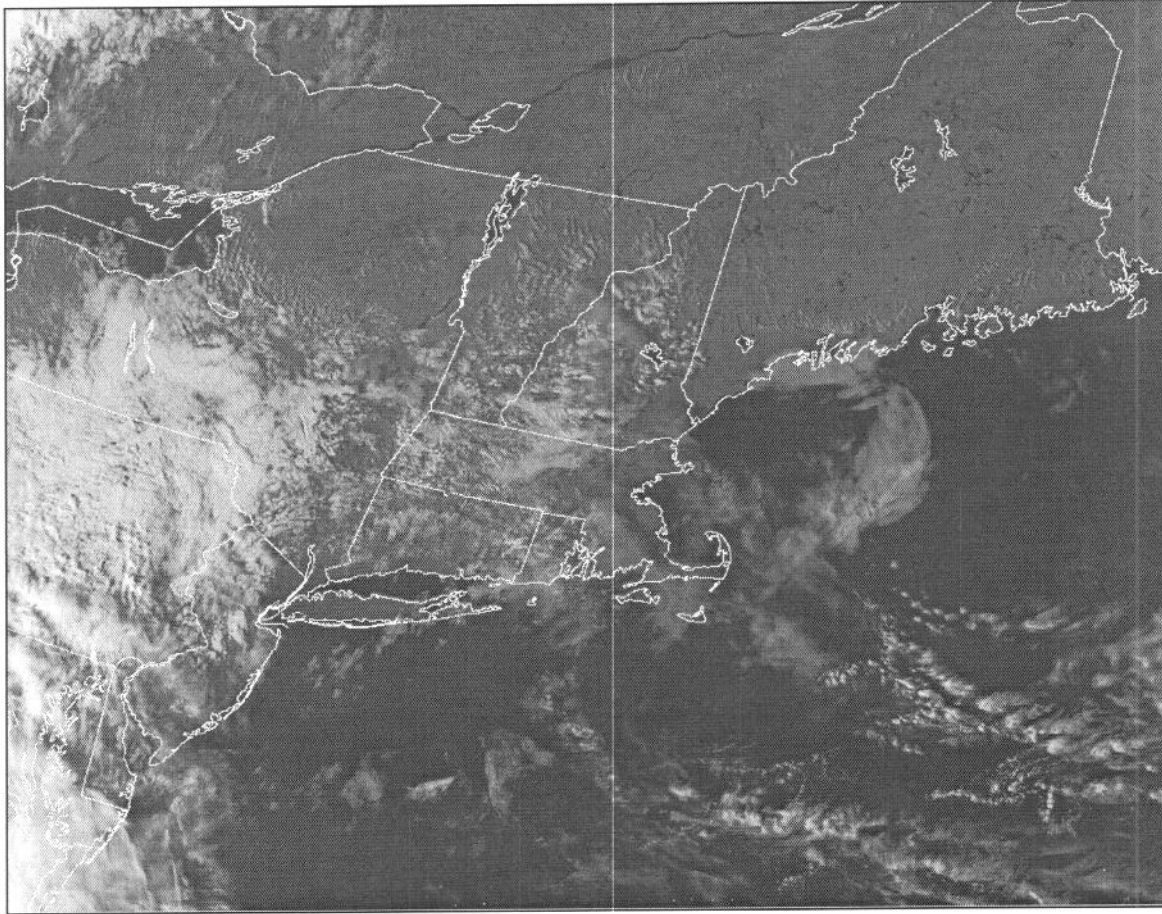


Figure 2. AVHRR channel 2 (0.86 μm) image of the New England and southern Quebec region at 1928 UTC on 28 September 1999 used in terminator scene generation

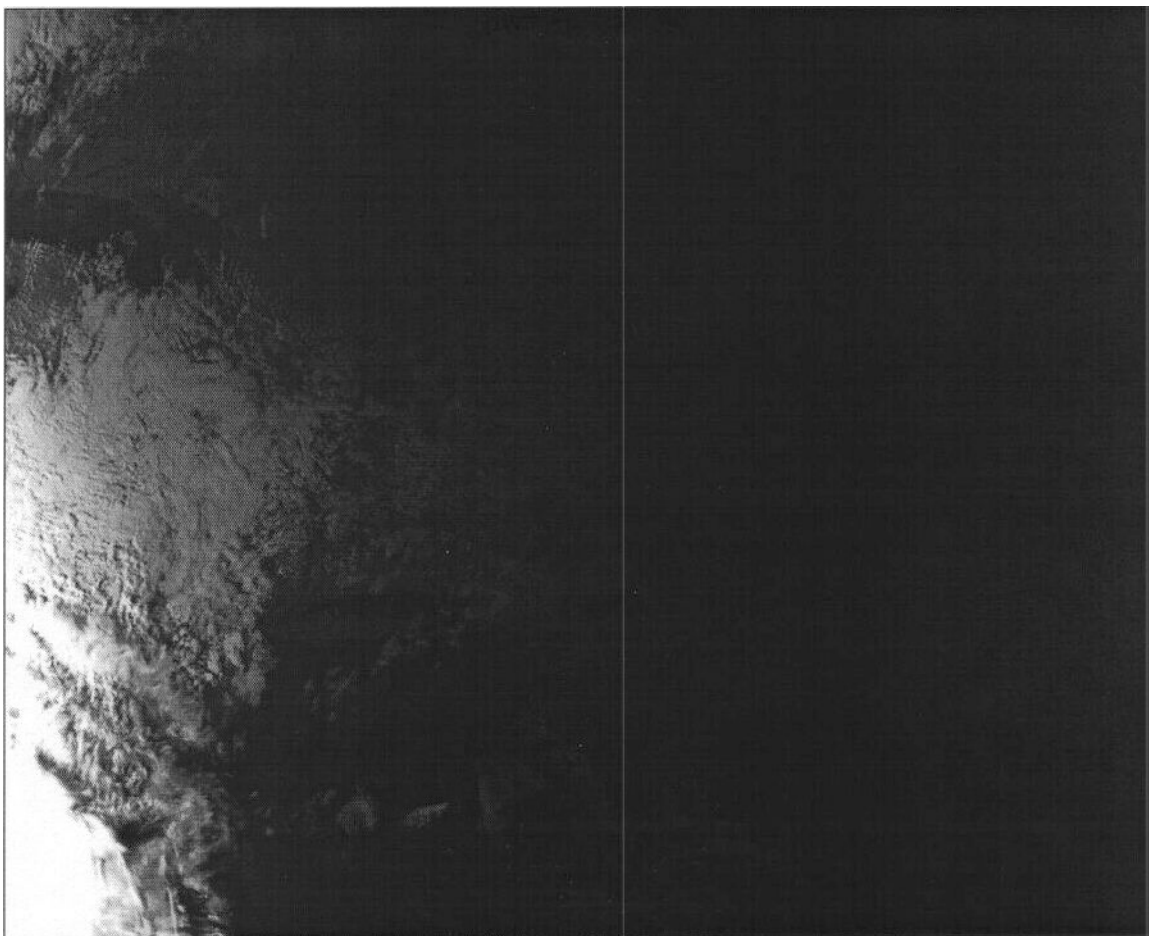


Figure 3. AVHRR channel 2 ($0.86\ \mu\text{m}$) terminator scene generated with base image from Fig. 2

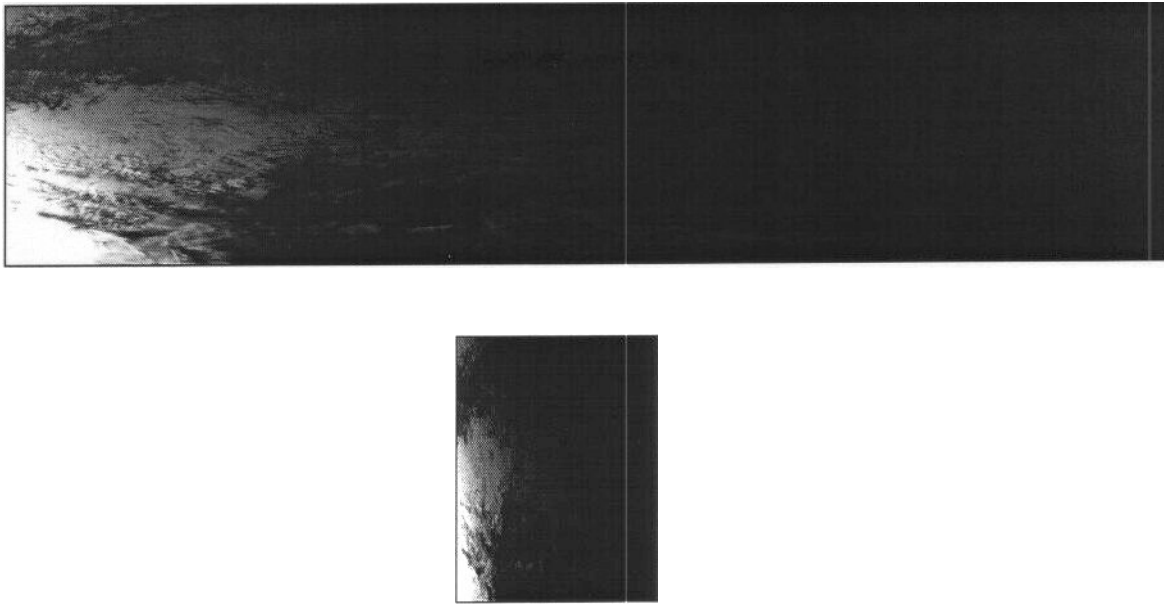


Figure 4. Low-light band terminator image in instrument coordinates at nadir (top) and at edge of field (bottom) after application of the simple sensor effects model

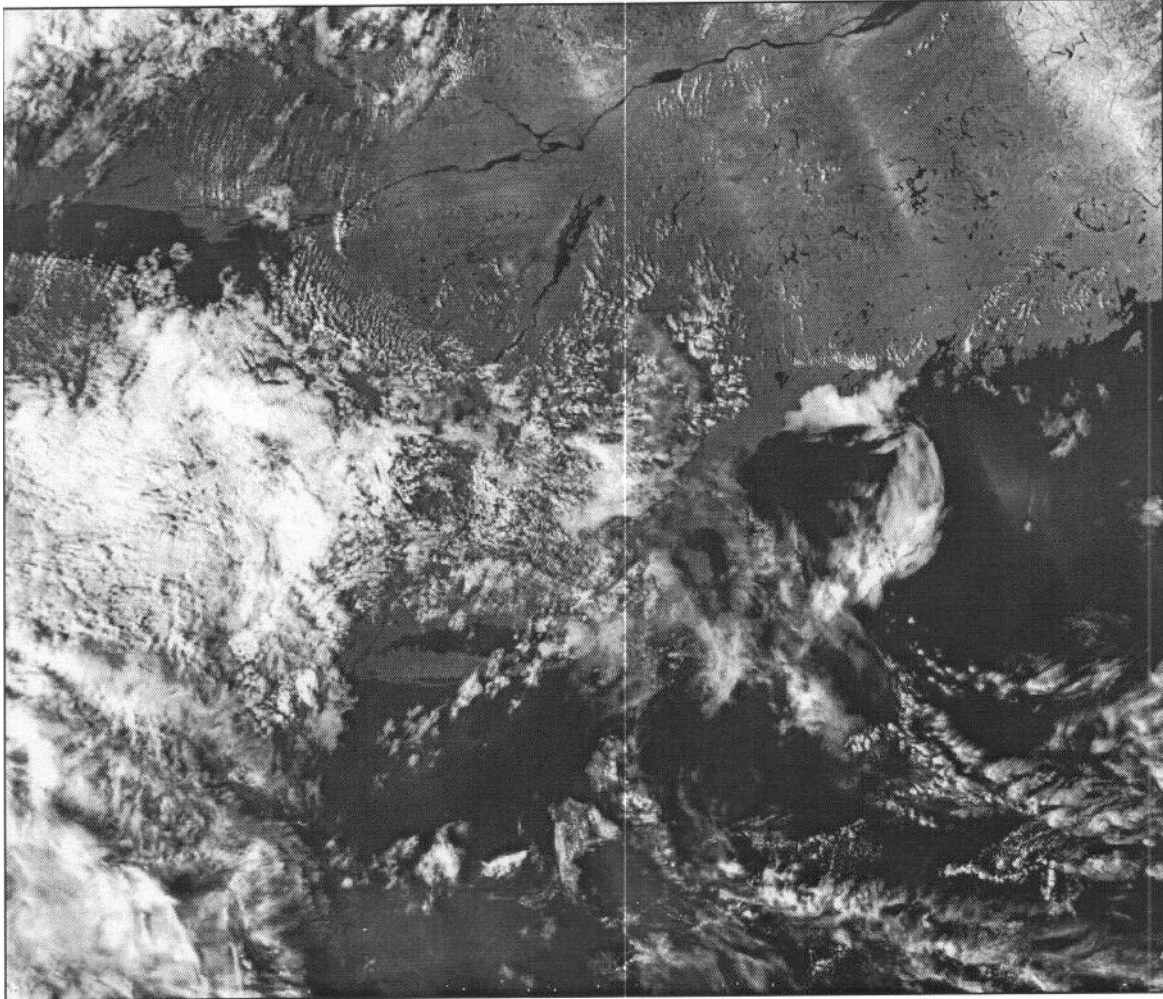


Figure 5. NCC product for low-light band nadir scene remapped to a 1.47 x 1.47 km grid. Bin width is 0.5 SZA degree; bin length is 1/10th the (N-S) length of the image.

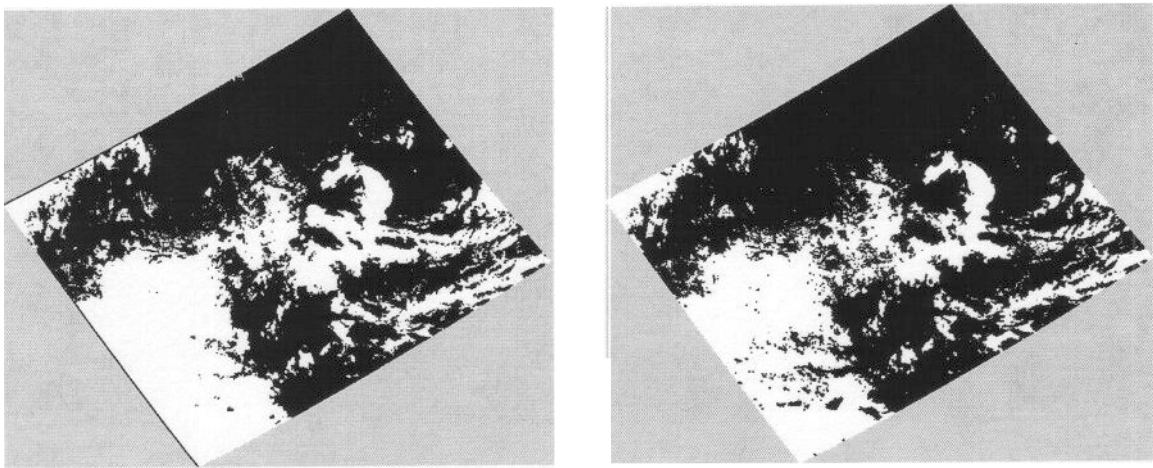


Figure 6. Manually analyzed cloud masks from AVHRR data (left) and NCC product (right) each remapped to a common Lambert equal area map projection



- [Ship Inside U.S.](#)
- [Ship Outside U.S.](#)
- [Ship Inside U.S.-Freight](#)
- [Ship Outside U.S.-Freight](#)
- [Track Shipment](#)
- [Cancel Shipment](#)
- [Schedule Courier](#)
- [Address Book](#)
- [Fast Ship Profiles](#)
- [Shipping History](#)
- [Report Manager](#)

- [Update Shipping Profile](#)
- [Help/FAQs](#)
- [Tutorial](#)
- [Contact Information](#)

- [My Profile](#)
- [Go to fedex.com](#)
- [Go to My FedEx](#)
- [Go to Ship Manager Login](#)

- [Order Supplies](#)

- [Logout](#)

Your Shipment Details

Tracking Number: 790499710368 **Date:** Jul 26 2002

From:
 Jenny Moore
 NOAA/INTEGRATED
 PROGRAM OFFICE
 8455 COLESVILLE ROAD
 SUITE 1450
 SILVER SPRING MD 20910

US
 3014272084

To:
 SAF/PAS
 1690 Air Force
 Pentagon -5D227
 Washington DC
 20330
 US
 703-697-9542

Service: Standard
 Overnight
Packaging: FedEx Box
Pickup/Dropoff: Drop Off
Handling:
Dimmed: 0 X 0 X 0

Weight: 1LBS
Shipper Account Number:
 171766664
Bill Shipment To:
 171766664

Bill Duty/Tax/Fees: 0
Express Reference:
Declared Value: USD0
Status: N/A

Courtesy Rate Quote*:**
 4.51
COD Amount: N/A

*The courtesy rate shown here may be different than the actual charges for your shipment. Differences may occur based on actual weight, dimensions, and other factors. Consult the applicable FedEx Service Guide or the FedEx Rate Sheets for details on how shipping charges are calculated.

[Schedule Courier](#)
[Find a Dropoff Location](#)
[Shipping History](#)
[Ship Inside U.S.](#)
[Ship Outside U.S.](#)
[Ship to Same Recipient](#)

02 - 0484
Call 697-3222/697-8932
for pickup or return to 5D227

Scene Generation Studies in Support of the Next-Generation of Polar Orbiting Low-Light Imagers

George D. Modica*, Edward J. Kennelly, John Evans, Robert P. d'Entremont,
Gary B. Gustafson

*Atmospheric and Environmental Research, Inc.
131 Hartwell Ave.
Lexington, MA 02421*

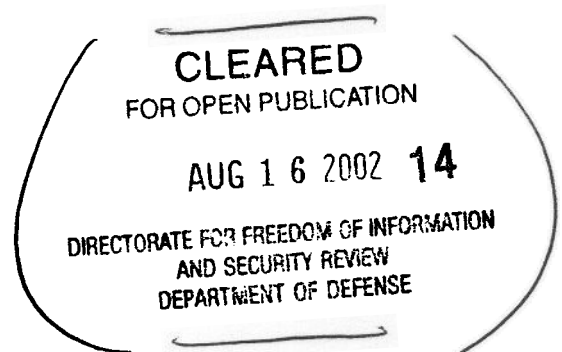
David E. Flittner

*Dept. of Atmospheric Sciences, University of Arizona
Tucson, Arizona*

Neil Endsley

*Ball Aerospace Corporation
Boulder, Colorado*

5 October 2001



* Corresponding author address: George D. Modica, AER, Inc., 131 Hartwell Ave., Lexington, MA
02421-3126. Email: gmodica@aer.com
Current affiliation: University of Maine

02-52341

ABSTRACT

We describe a process to synthesize satellite imagery that exhibits characteristics similar to what might ultimately become available from the nighttime visible band of the next-generation of polar-orbiting imager instruments. The process begins by creating a modeled scene that includes a realistic terminator—the region where the magnitude of the top-of-atmosphere radiance is a strong function of the solar zenith angle. The terminator is accurately modeled by first obtaining data from a spherical coordinate multi-scattering radiative transfer model. Only the moon in quarter-phase illuminates the nighttime side of the terminator. After this data is applied to the scene, the effects of instrument motion blur, resampling, noise, etc. are parameterized and introduced into the image through the use of a simple sensor effects model. The simulated terminator imagery is used to test a Near Constant Contrast (NCC) algorithm that is supposed to produce an image in which, among other things, the contrast of scene features does not vary noticeably anywhere along a line transiting the terminator. The NCC product generated by this algorithm compares favorably with the original ground truth image used as the basis for the modeled terminator scene in terms of feature validation achieved through a manual analysis of the imagery. This exercise raises the level of confidence in the capability of a prospective NPOESS nighttime visible band instrument to provide data that will satisfy user-driven requirements and be of great benefit to operational and research meteorology.

1. Introduction

The launch of the first Television Infrared Observation Satellite (TIROS) was the United States' first experimental milestone to determine the usefulness of satellites to study the earth. Over forty years later, the role that weather satellites fulfill has never been greater and new systems continue to be designed, developed, and launched into service. On the 40th anniversary of TIROS, it is appropriate to recount a few of the environmental issues that have benefited as a result.

Recognizing the crucial role that clouds play in global climate, researchers have relied on cloud and ice analyses derived from satellite image data to provide clues to the mysteries of global-climate change. Population growth and "urban sprawl" are objectively monitored by examination of time series satellite data of city lights. Satellite imagery also provides a real-time means of monitoring man-made and natural fires, natural gas field flaring, land use, severe weather, and aurora to name a few.

The current inventory of operational polar-orbiting imaging satellites that have contributed to these achievements each have their roots in programs from one or more of three agencies: NASA, NOAA, and the Defense Meteorological Satellite Program (DMSP). NASA, e.g., has led the development of the Landsat Thematic Mapper (Tokola et al. 1999). This is a multispectral imager that provides high spatial resolution information on land use. It has a horizontal spatial resolution of 30 m at nadir. More recently, NASA launched the Moderate Resolution Imaging Spectroradiometer (MODIS), which acquires imagery at up to 250 m resolution for a much wider swath width than Landsat. The Advanced Very High Resolution Radiometer (AVHRR; Rao et al. 1990) sponsored by NOAA is a 5 channel scanning radiometer with 1.1 km resolution. The DMSP Operational Line Scan (OLS; Kroehl et al. 1994) is another imaging instrument that consists of two telescopes: one for the visible band and one for IR, each

having 0.55 km horizontal spatial resolution. The OLS includes a nighttime visible capability—something not present aboard the civilian platforms—having 2.7 km horizontal spatial resolution and is made possible through the use of photo-multiplier tube (PMT) technology. The PMT is sensitive to very low levels of light in the 0.47-0.95 μm band, enabling detection of meteorological features with as little as half-moonlight illumination. The nighttime visible imaging feature of the OLS is important for extending visible-band analysis capability into non-daylight hours. While IR channel data is essential for nighttime viewing, under certain conditions (e.g., strong temperature inversions, transmissive clouds) image features can be more difficult to interpret. In fact, the nighttime visible band data is so useful that it was added to the requirements for the National Polar-orbiting Operational Environmental Satellite System (NPOESS), which is discussed in Section 2. It is our interest in the “low-light” imaging requirement of NPOESS that motivated this study. Having the ability to experience beforehand the imagery characteristics provided by a new low-light instrument is, of course, desirable in itself. But it is also an essential component in the design phase of an imaging instrument as it not only affords potential users of the data the opportunity to test and refine ahead of time algorithms that might potentially use the data, but assists the instrument designers as well. In Section 3 we present a methodology to generate the desired imagery product followed by a discussion in Section 4 of the results produced by an algorithm that used the imagery.

2. NPOESS

NPOESS combines the country’s civilian and military weather polar-orbiting satellite programs into a single system. NPOESS is currently in the development phase and will begin to provide data operationally in the 2005-2008 time frame. There are 6 NPOESS payloads currently under development: the Visible/IR Radiometer Suite (VIIRS), the Cross-track IR Sounder (CrIS), the Conical Microwave Imager/Sounder (CMIS), the Ozone Mapper/Profiler Suite (OMPS), the GPS Occultation Sensor (GPSOS), and the Space Environmental Sensor Suite (SESS). NPOESS is intended to provide *operational* remote sensing capability to acquire and receive environmental data in real-time. The data will be acquired at field terminals and acquired, stored, and disseminated at processing centers. The environmental data will consist of global and regional imagery, specialized meteorological, climatic, terrestrial, oceanographic, and solar geophysical data in support of both civilian and national security missions.

A key strategy of NPOESS is to optimize the development of critical sensor payloads through the unprecedented participation of the algorithm developer in the sensor design process. Rather than develop algorithms *after* the instruments have been designed, algorithm developers are involved in all phases of instrument development: requirements analysis, design, testing, and evaluation of the sensors, measuring performance against end-user requirements each step of the way. Algorithm development is primarily driven by formal NPOESS specifications, which include requirements for the system to produce specific Environmental Data Records (EDRs). EDRs are data that contain the measured environmental parameters or imagery as well as any ancillary data required to identify or to interpret these parameters or images. EDRs are generally produced through the application of one or more algorithms to the Sensor Data Records (SDRs) and must meet specific content, quality, reporting frequency, and timeliness requirements.

angles (Herman et al. 1995). In this model, the atmosphere is divided into homogenous spherical shells. The intensity at any point is a function of five independent variables (3 for location and 2 for the direction of radiation). The model parameterizes the effects on radiative transfer of aerosol scattering, gaseous and aerosol absorption, and in more recent versions, polarization. For each shell, the model uses an integrated form of the general radiative transfer equations and computes all distances and angles by assuming spherical geometry.

Previous tests of this model indicated it is accurate to better than 1% for most Earth-atmosphere situations. When compared with “flat” or plane parallel atmospheric models, differences > 10% were found in the transmitted intensities at the surface for all lines of sight when the SZA was greater than 85° and spherical effects were neglected. For an optical depth of 0.5, a SZA > 80°, and view angles within 10% of the horizon, spherical effects must be included to avoid errors greater than 5%. For a SZA of 85°, errors of 5% were found for optical depths as small as 0.1. Other comparisons of the spherical geometry model with the flat model confirm the need to include spherical effects when examining the intensity field at the top of the atmosphere.

We used this model to expose some of the performance implications of a visible band low-light sensor that images from a low earth orbit (~833 km) in the vicinity of the terminator. For this study, the RTM was used to estimate effective TOA normalized (I/F) scene reflectance as a function of the conditions specified below in Table 1. Table 2 lists the surface parameters used in the model. The results from the RTM are generally consistent with earlier Air Force data that describe the drop in TOA radiance with increasing SZA at OLS/PMT visible-wavelengths (Figure 1). Some quantitative differences between the OLS and RTM curves were bound to occur due to assumptions on the control parameters listed below. Nevertheless, it will be invaluable from the standpoint of both algorithm and instrument design if the RTM can be used to provide quantitative guidance on the nature of scene radiances in the vicinity of the terminator.

Table 1. Satellite and solar geometry parameters

Parameter	Value
Wavelengths ¹ (nm)	469
	542
	645
	858
Solar Zenith (deg)	105
	100
	95
	90
	85
Satellite Zenith (deg)	0
	45
	70
Azimuth ² (deg)	0 to 150 (every 30 deg)
	150-180 (every 5 deg)

¹Wavelengths selected to match center wavelengths of VIIRS bands.

² Azimuth angle convention is such that 180° indicates sensor looking directly toward sun, 0° is satellite directly between sun and viewed point.

Table 2. Surface type parameters

Surface Type	Reflectance				Altitude (km)
	469 nm	542 nm	645 nm	858 nm	
vegetated land	0.07	0.10	0.07	0.40	0
ocean	BRDF	BRDF	BRDF	BRDF	0
cloud	0.70	0.70	0.65	0.65	2

b. Input scene selection

Unfortunately, VIIRS imagery will not be available for several more years. In order to test VIIRS algorithms in the meantime, the VIIRS imagery must be approximated. In making these approximations, several important issues must be addressed.

The first issue in scene approximation or generation is that it is necessary to include the effect the sensor instrument has on the imagery. The instrument's electronic, optical, and mechanical components combine in characteristic ways to introduce artifacts into an image. Some of these sensor characteristics are commonly known as sensitivity, noise, out of field effects, spatial smoothing, and distortion. Any attempts to approximate VIIRS imagery must account for and include these effects. The effects can be simulated with the use of a sensor model that can parameterize these characteristics to approach the VIIRS specifications. A second issue is the attenuation of radiances from clouds (water and/or ice) and by the intervening atmosphere. This effect has scan angle dependence, since the imager will view through a longer optical path at higher scan angles. A third complication arises when simulating cloud and ice features: Synthetic data with realistic spatial detail are extremely difficult to produce. In contrast to automated algorithms, analysts rely primarily on spatial—as opposed to radiometric—characteristics to interpret a scene. While radiative transfer models do exist to simulate accurately the radiometric characteristics of simplified cloud and terrestrial surfaces, the process of modeling scenes having complicated spatial features presents a much greater challenge.

The solution we adopted was to use a combination of high-resolution image data and sensor effects modeling (see below) as the basis for establishing our synthetic scene. This approach ignores the radiometric dependence on scan angle mentioned in the second consideration above, but for manual analysis applications where radiometric accuracy is not strictly required, this drawback is of second order importance. Of the imager platforms mentioned in Section 1, the AVHRR instrument aboard the NOAA polar-orbiting satellites was the most readily obtainable. While its horizontal spatial resolution is significantly less than that of Landsat, (1.1 km vs. 30 m at nadir) AVHRR provides a much larger swath width (2400 km vs. 185 km)—a useful advantage for simulating a scene that includes the full extent of the terminator region.

c. Terminator scene generation

In order to test the NCC product algorithm with imagery it will be necessary to collect candidate terminator scenes for input. As discussed earlier, obtaining real data for this purpose is problematic. However, we may use the RTM data to generate artificial terminator scenes by modulating the observed top-of-atmosphere (TOA) radiances from AVHRR *daytime* scenes, such that the resulting values decrease with increasing SZA in accordance with one of the curves from Figure 1. For this we selected a mid-afternoon AVHRR scene from September 1999 (Figure 2). The original field of SZA in this scene was replaced with values consistent with a terminator in the center of the scene. The next step was to modulate the TOA radiance values at every pixel to be consistent with the RTM curves for AVHRR channels 1 and 2. Model parameters appropriate for an assumed vegetation-covered surface (Table 2) were used. Since we had data from the RTM model at only five solar zenith angles from 85° to 105°, we interpolated the data with a cubic spline function to a lookup table at every 0.01 SZA degree. Next, we normalized the RTM curves so that the normalized radiance = 1 for SZA = 85°, essentially creating a table of weights as a function of SZA. Then, the radiance in the terminator scene (R_{term}^{ij}) was computed according to

$$R_{term}^{ij} = R^{ij} \cdot w(SZA), \quad (1)$$

where i, j are the indexes in the image x, y directions, respectively; R^{ij} is the initial AVHRR scene radiance; $w(SZA)$ are the weights obtained from the above look-up table.

Figure 2 shows the AVHRR scene used to provide R^{ij} . This image covers an area over the northeast United States and Atlantic Ocean. Some identifiable surface features in this image are the New England coastline and much of Long Island. The St. Lawrence River (with Lake Champlain to the south) may be identified near the top of the image, leading to its source—Lake Ontario—in the upper left. A variety of low-, mid-, and upper-level clouds cover much of the western edge and center of the image; clusters of clouds are also apparent over the Atlantic Ocean, with fog off of the coast of Maine. The field of R_{term}^{ij} , after application of the RTM curves to the AVHRR channel 2 data, is shown in Figure 3. Note that despite the apparent lack of identifiable features in much of the scene, there are in fact radiance variations. The scene radiances fall to about $9 \times 10^{-9} \text{ Wcm}^{-2}\text{sr}^{-1}$ in the 0.46 – 0.86 μm band (see below) over the darkest portion of the scene.

d. Spectral matching

The spectral resolution of the low-light band (assumed here to be 0.46 – 0.86 μm) is relatively broad with respect to the AVHRR channels in the same range (0.58-0.68 μm for channel 1 and 0.725-1.10 μm for channel 2). We may combine narrower band image data to produce a broader band image by using a spectral matching technique:

$$\bar{R} = \frac{\sum_{i=1}^2 a_i R_i}{\sum_{i=1}^2 a_i} \quad (2)$$

where R_i are the AVHRR channel radiances and a_i are weighting coefficients. The coefficients a_i were specified to be proportional to the AVHRR 50% power half-bandwidths. AVHRR channels 1 and 2 were used in Eq. 2.

e. Simple sensor effects model

There are many attributes of an image sensor that are important for image quality. The optics, mechanics (including properties of the orbit), and electronics of the imaging system can affect these attributes. Since our goal is to generate the most realistic NCC product as is reasonably possible, the synthesized scene used as input for the NCC algorithm ought have characteristics that are consistent with the low-light imager. We used a simple sensor effects model (SSEM) to do this. The SSEM includes parameterizations of the following effects:

- Horizontal Spatial Resolution (HSR)—a measure of the “sharpness” of the imagery. In the SSEM, this is determined by a choice of a system modulation transfer function (MTF), which is the Fourier transform of the end-to-end system point spread function (PSF). The SSEM includes the option to use different shaped PSFs (e.g., square, Gaussian);
- Horizontal Reporting Interval (HRI)—the ground space distance between neighboring points in the horizontal at which imagery is estimated and reported. Various combinations of under- or oversampling may be tested. For reasons that are beyond the scope of this paper, we selected an NCC grid having a 1.47 x 1.47 km pixel dimension to satisfy the HSR and HRI requirements.
- Noise—artifacts introduced into an image due to system imperfections. Noise affects the uniformity of the target and background and the potential for differentiating between them (i.e., contrast). Sources can be coherent (correlated) and incoherent (random, e.g., white noise). This also includes quantization noise, which arises from the discretization of the dynamic range of an instrument as determined by the number of bits used to quantify the radiance. Noise models developed for the VIIRS low-light instrument were utilized in the sensor simulation.

The simple sensor effects model is not intended to be a substitute for rigorous modeling of all sensor system effects. The formal design process of the low-light visible band instrument included the development of a sophisticated sensor system model that explicitly represents every component of the imaging system. However, the SSEM ensures that the most stressing low-light band image quality effects are accounted for. These are pixel aspect ratio, MTF, and HRI. While the original AVHRR scene (Figure 2) used as input to the SSEM includes its own unique sensor artifacts, we believe these do not detract from the results in this study for the following reasons: Most importantly, the NCC product is not a radiometric product at all, since there has to be a transformation from radiance space to “gray-shade” space during contrast adjustment (see Section f below). Were we primarily interested in the absolute radiometry of the low-light band, we would have to be more sensitive to the AVHRR sensor effects. Secondly, the AVHRR and low-light band pixel sizes at nadir are smaller than the 1.47 x 1.47 km pixel

dimension of the NCC grid. Minimally detectable spatial features that would be most affected by characteristic AVHRR sensor effects will be all but lost when sampled to the NCC grid.

Figure 4 shows the scene in the sensor coordinates of the low-light imager. The figure presents the results from two cases: The top figure shows the view based on the shape of low-light band pixels at nadir, while the lower figure shows the scene is based on edge of field shaped pixels. The reason the aspect ratio of the scenes differs from that in the original (Figure 3) is because of the low-light sensor pixel shape, which at nadir is rectangular, with the along-track dimension about three times the cross-track value. At edge of field (1500 km from nadir) and since this particular sensor design was a push-broom type instrument, the pixel aspect ratio changes to one having a cross-track width twice that of the down-track length. These characteristics were based on an 833 km altitude orbit.

f. Contrast adjustment

Since nighttime visible imagery band data can span a very large dynamic range (over seven orders of magnitude; see Figure 1), visual display of the data presents a challenge because common display techniques are best suited to viewing data that typically spans no more than two orders of magnitude. To meet requirements, a contrast normalization data processing step is necessary to ensure that the NCC data will be presented in a way that ensures adequate contrast across all radiance levels expected in the image. The contrast normalization is most effectively carried out locally, i.e., over a subset of the entire image to accommodate the potentially wide dynamic range of scene radiances. An adaptive algorithm whose parameters change from pixel to pixel according to the image contrast of local, or neighboring pixels may be used to achieve the desired enhancement. One such algorithm has been described in Schowengerdt 1997, and is known as Local Range Modification (LRM). The algorithm partitions the image spatially into adjoining bins. Due to the fact that the brightness intensity of the image can be a strong function of SZA (Figure 1), we modified the LRM algorithm to align the long axis of each bin parallel to lines of constant SZA. The bin dimensions are adjustable: The bin width is selected as a function of the SZA and the bin length as a function of the image (height) dimension. The algorithm next computes a contrast stretch unique to each pixel. This stretch is dependent on the local contrast within bin n ($n = 1, 2, 3, \dots, N$ number of bins per image):

$$GL_{i,j}(n) = 255 * \frac{(DN_{i,j} - DN_{min})_n}{(DN_{max} - DN_{min})_n}, \quad (3)$$

where $GL_{i,j}(n)$ is the gray level for pixel i,j within bin n , $DN_{i,j}$ is the digital number of pixel i,j , and $(DN_{min} - DN_{max})_n$ is the digital number range in bin n . Here, we assume the display ranges from [0, 255] gray shades.

4. Results and Discussion

a. Qualitative aspects of the NCC product

The NCC product is shown in Figure 5. The nadir image in Figure 4 was used as input to the NCC product algorithm. The NCC algorithm regrid the image from the low-light instrument scan projection of Figure 4 to the 1.47 km NCC product grid and performs the contrast adjustment with Eq. 3. There were few noticeable differences between the nadir NCC product and a second one (not shown) that used edge of field-shaped pixels. A comparison of the NCC product with the original AVHRR terminator scene in Figure 3 reveals that the most obvious difference is in features within the “nighttime” region; clouds and surface features are now readily identifiable in the NCC product, as they are in the original AVHRR image (Figure 2). A closer look also supports the claim that the contrast is not a function of position with respect to the terminator. However, Figure 5 does present an example of how artifacts can be introduced into the image by the LRM algorithm. In the northeast corner of Figure 5 in the vicinity of the St. Lawrence River, some of the bin boundaries are noticeable. These appear as striping oriented northwest-southeast in the image. The striping is caused by the tendency of the LRM technique to distribute the contrast in a bin across all [255] gray shades even when there isn’t much contrast to begin with (i.e., the denominator in Eq. 3 is small). Unfortunately, without supporting information such as snow cover analysis, or some other meteorological guidance, this artifact could be misinterpreted as cloud or snow cover. To a lesser extent, bin boundaries are also evident over the Atlantic Ocean, south of Long Island. It should be noted here that the NPOESS user workstations would likely be configured with a wide variety of supporting databases to assist in the identification of features of interest. Furthermore, in an operational setting at a field terminal, a user likely would be able to manipulate easily the choice of bin size used in the LRM algorithm. In fact, tests have revealed that with a little trial and error, undesirable artifacts in the NCC product can be minimized to an acceptable level for manual applications. Lastly, future versions of the NCC algorithm itself could include refinements that will minimize the introduction of artifacts for those regions in the scene having little contrast.

b. Quantitative aspects of the NCC product

The NCC product was intended to provide users with an additional nighttime information source for analyzing imagery. In order to guarantee that sufficiently high quality imagery will be available from the low-light band sensor aboard VIIRS, both instrument and algorithm designers must demonstrate that this imagery meets certain threshold requirements. As mentioned in Section 2, certain of these requirements are applicable to the content, quality, reporting frequency, and timeliness of the imagery; others pertain to specific, manually derived products that are based upon the imagery. Some examples of the latter are cloud cover fraction, cloud type, sea ice concentration, and sea ice edge location. These products can be derived using any combination of VIIRS imagery bands, display enhancements, and additional supporting databases, such as geography. The requirements for the manually derived cloud cover fraction product are shown in Table 3. These and other requirements are detailed in a Systems Requirements Document issued by the NPOESS Integrated Product Office.

Parameter	Thresholds	Objectives
a. Horizontal Cell Size	3 times the Imagery HSR	2 times the Imagery HSR
b. Horizontal Reporting Interval	Horizontal cell size	Horizontal cell size
c. Measurement Range	0 - 1, 0.1 increments	0 - 1, 0.1 increments
d. Measurement Uncertainty	0.1	0.1

Table 3. Requirements for manually the derived cloud cover fraction product

The Horizontal Cell Size (HCS) in Table 3 refers to the areal extent of an image sample in which we wish to measure cloud fraction. In this case, the HCS is defined as “3 times the [VIIRS] Imagery HSR,” which is 3 times 400 m, or 1.2 km. Therefore, the problem becomes one of determining the fraction of a $(1.2 \text{ km})^2$ area covered with cloud. The Horizontal Reporting Interval (HRI) specifies how frequently (in space) the cloud fraction is to be reported. In this case, the HRI is equal to the HCS. This implies the analyzed cells must be contiguous. The Measurement Range specifies the interval at which the cloud fraction must be analyzed (i.e., 0, 0.1, 0.2,1.0). Finally, the Measurement Uncertainty is a measure of error and indicates how far the manually derived cloud fraction departs the actual, or truth value. The measurement uncertainty is defined as

$$\xi_N = \left[\sum_{i=1}^N (x_i - x_T)^2 / N \right]^{1/2} \quad (4)$$

where x_i is the value obtained in the i th estimate of the parameter, and x_T is the truth value of the parameter. The value of ξ_N is required to be ≤ 0.1 . It is important to note that the NCC product does not by itself have to meet the measurement uncertainty requirement given in Table 3; rather, a manual analysis may be derived from any or all of the imagery channels. These include daytime visible and thermal infrared channels having 400m HSR (nadir).

Since we are interested in learning some of the characteristics of the NCC product, we computed the cloud fraction measurement uncertainty as defined in Eq. 4 based only on the NCC product shown in Figure 5. We used the following procedure to enable us to make this calculation: First, we produced a manual cloud analysis from the NCC product image shown in Figure 5 to yield a cloud mask. For this we utilized a “threshold blanking” utility that permits adjusting downward the intensity of the background over some subset of the full scene until only the target (e.g., the clouds) remains. The subset area is saved, and the process is repeated until the entire scene is covered. The result is a yes/no cloud mask for each pixel of the NCC product. A second manual cloud analysis from a similar procedure was produced by using the full (5) channel set of the higher spatial resolution AVHRR “truth” image shown in Figure 2. In this case, we also utilized visualization tools that permitted multispectral enhancement of the truth imagery. Note that we generated the NCC product cloud mask *before* the truth mask, so as not to prejudice the former. Since the AVHRR data and NCC product exist on different grid projections (AVHRR is in scan projection and the NCC product is on a $1.47 \times 1.47 \text{ km}$ grid), the third step in the processing required remapping the cloud masks from each analysis to a common grid. We selected for this test a Lambert Equal Area map

projection. The remapped cloud masks from the truth analysis and NCC product are shown in Figure 6. Finally, Eq. 4 was applied to the data in Figure 6 to calculate the measurement uncertainty. In this test, we obtained a measurement uncertainty value of 0.23. While this is certainly greater than the threshold value of 0.1 given in Table 3, it is reasonable after considering that the manual cloud fraction analysis used no sources of information other than the NCC product. During the test phase of VIIRS we routinely achieved the threshold requirement for cloud cover measurement uncertainty when the higher spatial and spectral resolution VIIRS imagery data were available.

In this study, we simulated imagery from an as-yet-to-be-built low-light band satellite sensor as a means of supporting the risk reduction activities during the design phase of the NPOESS VIIRS program. The simulated imagery exhibits the essential characteristics we expect to see in real satellite data. We used this simulated imagery to test an NCC product algorithm, which must be capable of displaying features down to quarter-phase lunar illumination conditions. A quantitative assessment of the NCC product suggests that it will be an invaluable component in cloud (or ice) analysis, not to mention climate, land use studies, and other applications.

Acknowledgments. This effort was supported by the NPOESS Integrated Project Office through a contract with ITT Defense and Electronics.

REFERENCES

- Herman, B., T.R. Caudill, D.E. Flittner, K.J. Thome, and A. Ben-David, 1995: Comparison of the Gauss-Seidel Spherical polarized radiative transfer code with other radiative transfer codes. *J. Appl. Optics*, **34**:13, 4563-4572.
- Kroehl, H.W., G.R. Scharfen, E.S. Arrance, and S.J. Goodman, 1994: Archive of digital data from the Defense Meteorological Satellite Program (DMSP). *Tenth International Conference on Interactive Information and Processing Systems for Meteorology, Oceanography, Hydrology*, January 23-28, Nashville, TN, American Meteorological Society.
- Rao, P.K., S.J. Holmes, R.K. Anderson, J.S. Winston, and P.E. Lehr, 1990: *Weather Satellites: Systems, Data, and Environmental Applications*. American Meteorological Society, Boston, ISBN 0-933876-66-1.
- Schowengerdt, R.A., 1997. *Remote Sensing; Models and Methods for Image Processing*. 2nd ed. San Diego, CA: Academic Press, 522 p.
- Tokola, T., S. Löfman, and A. Erkkilä, 1999: Relative calibration of multitemporal Landsat data for forest cover change detection. *Rem. Sens. Env.*, **68**:1, 1-11.

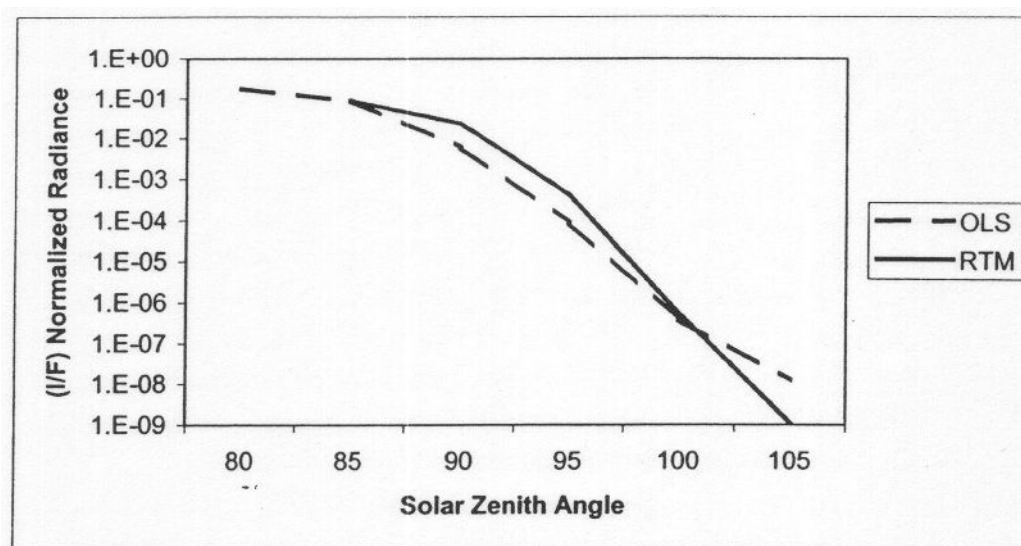


Figure 1. Normalized scene radiance as a function of solar zenith angle for OLS and the radiative transfer model (RTM)

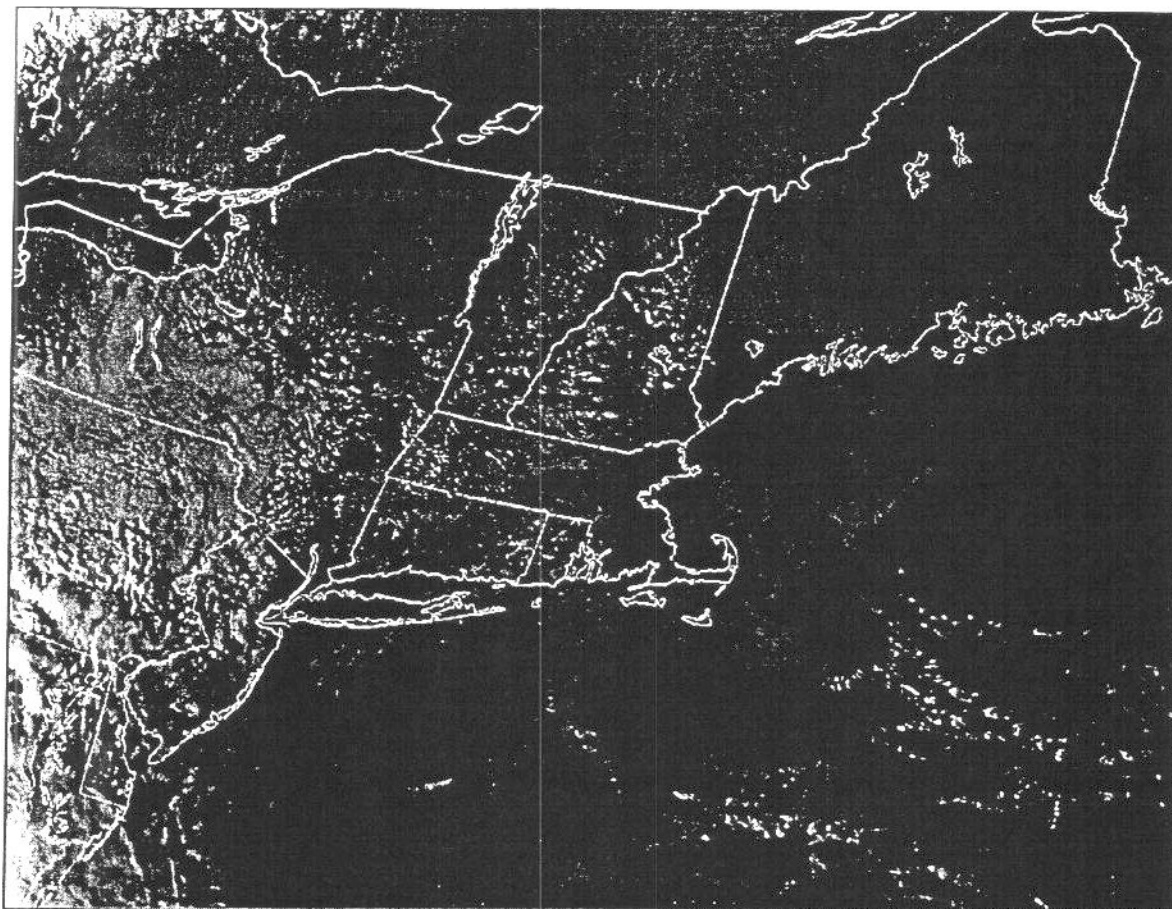


Figure 2. AVHRR channel 2 (0.86 μm) image of the New England and southern Quebec region at 1928 UTC on 28 September 1999 used in terminator scene generation

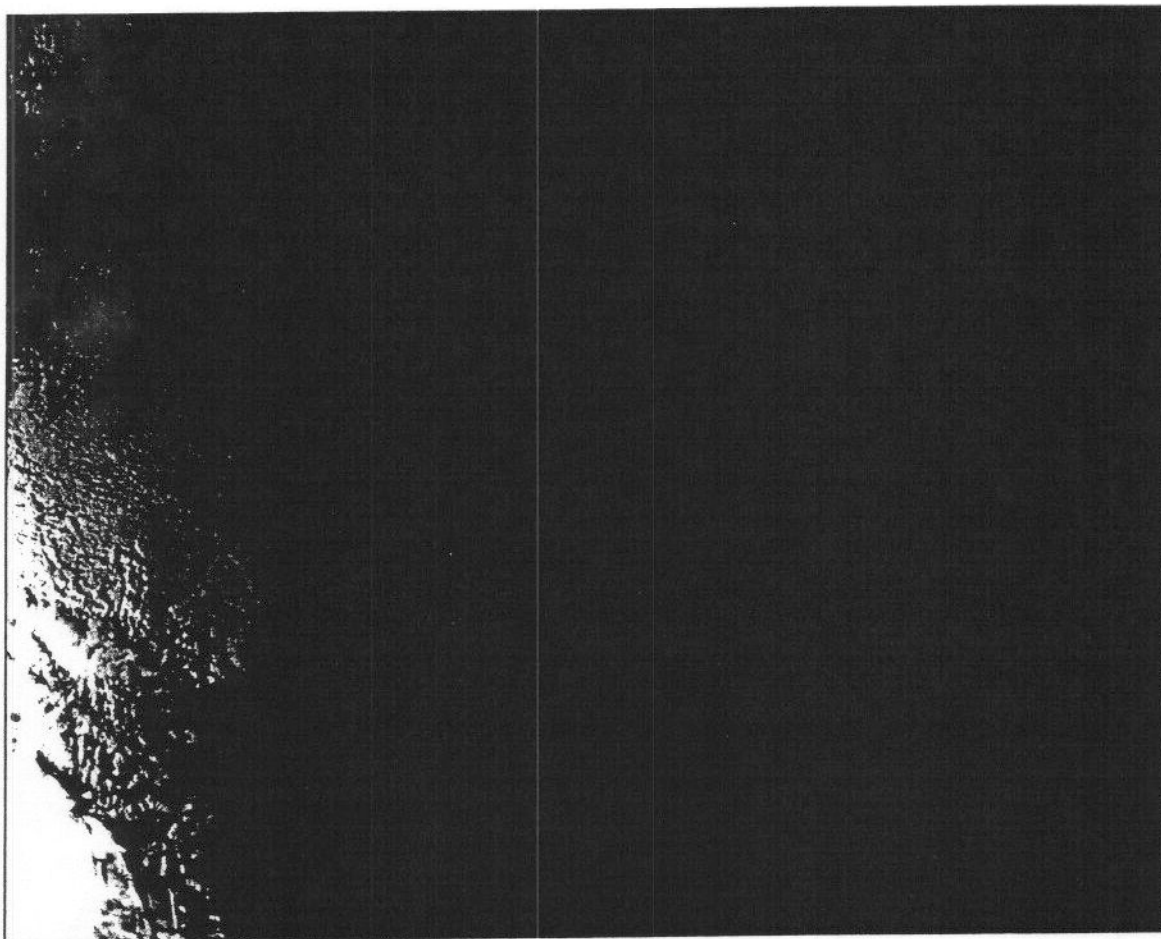


Figure 3. AVHRR channel 2 (0.86 μm) terminator scene generated with base image from Fig. 2

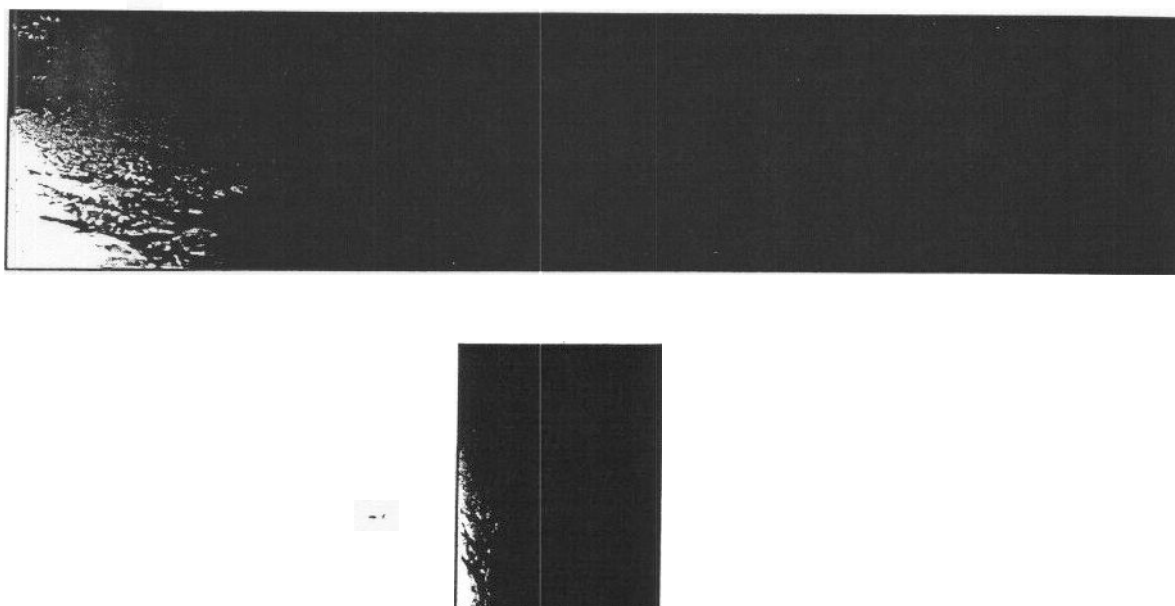


Figure 4. Low-light band terminator image in instrument coordinates at nadir (top) and at edge of field (bottom) after application of the simple sensor effects model

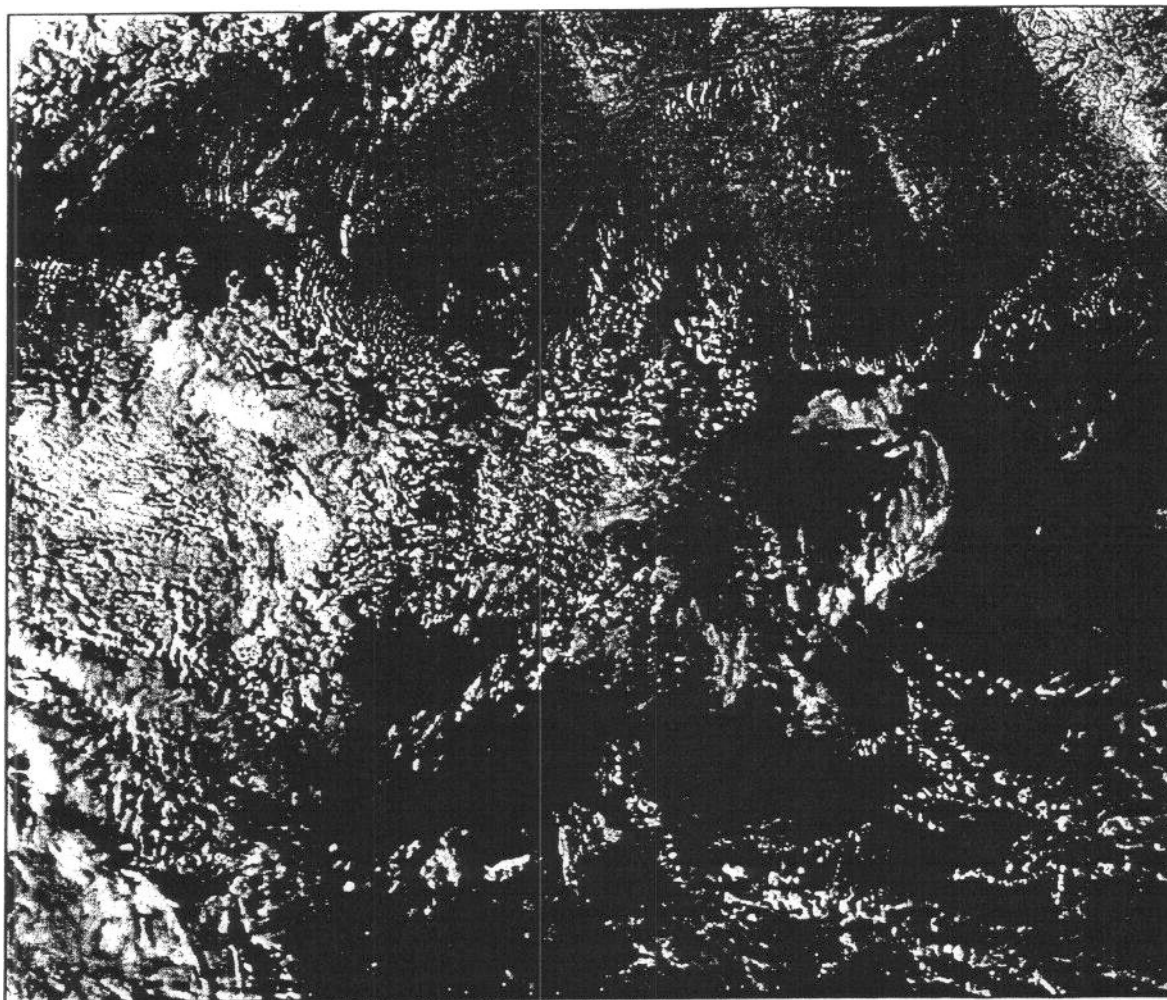


Figure 5. NCC product for low-light band nadir scene remapped to a 1.47 x 1.47 km grid. Bin width is 0.5 SZA degree; bin length is $1/10^{\text{th}}$ the (N-S) length of the image.

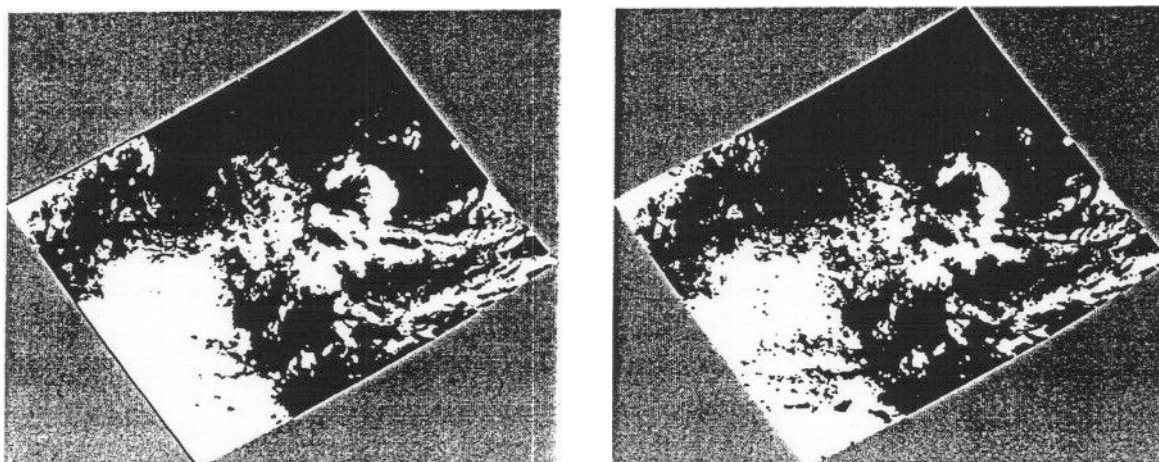


Figure 6. Manually analyzed cloud masks from AVHRR data (left) and NCC product (right) each remapped to a common Lambert equal area map projection